pathway over the short-term and only partially reset in the long-term (Jones and Thoren, 1977), which may account for sustained responses observed in the step protocol and dynamic protocol with high-voltage stimulation.

Methodological consideration

Fan and colleagues (Fan and Andresen, 1998; Fan et al., 1999) demonstrated that A-fiber baroreceptors were activated by low intensity (<3 V) stimulation and required minimum frequencies above 10 Hz to evoke reflex reductions in AP. In contrast, high stimulation intensities (20 V) maximally activated both A- and C-fiber baroreceptors, and high intensity stimulation decreased MAP at low frequency (1 Hz) stimulation. Furthermore, the application of capsaicin blocked the reflex response observed at high intensity and low frequency (Fan and Andresen, 1998). Reflex responses at supramaximal intensity during capsaicin were not significantly different from pre-capsaicin low intensity stimulation reflex responses (Fan and Andresen, 1998). Our findings are largely in agreement with the conclusions from Fan and colleagues.

The data from our graded frequency step stimulation protocol added new findings that low intensity stimulation of the ADN resulted in reflex responses that returned towards pre-stimulation levels after only 30 seconds of continuous stimulation. In contrast, high intensity stimulation resulted in sustained reductions in SNA and MAP, but after the application of RTX the responses became similar to those of low intensity stimulation. These data indicate that A-fiber baroreceptors, while being able to account for approximately 70–80% of the combined maximal reflex response to high-frequency stimulation in the study by Fan and Andresen (1998), only contribute to the reflex responses over a short time frame. Activation of C-fiber baroreceptor central pathways appears to be required to elicit reflex responses that are sustained throughout the duration of stimulation.

Based on the results of the step stimulation protocol, LVHf and HVLf dynamic stimulation protocols were devised to chiefly activate reflex response from A- and C-fiber baroreceptors, respectively. Note that although HVLf stimulation can activate both A- and C-fibers, the frequency is considered to be below the physiological threshold for recruiting the A-fiber central pathway (Fan and Andresen, 1998). Our data supports the rationale for selected stimulation protocols, because the central arc transfer functions obtained from LVHf stimulation protocol were largely unaffected by the application of RTX. In contrast, the HVLf stimulation protocol resulted in responses largely from C-fiber type baroreceptors as the application of RTX significantly reduced both dynamic gain and coherence of the central arc transfer functions.

Limitations

While the present study provides insight into how electrical activation of the arterial baroreflex relates to changes in SNA and AP there are some caveats to consider. First, action potential trains from electrical stimulation have a significantly different profile from those evoked by natural pressure stimulation of A- and C-fiber baroreceptors. Secondly, we investigated the responses to electrical stimulation of the ADN in anesthetized rats. Anesthesia may affect SNA, therefore, our results might differ had the experiments been performed in conscious animals. Furthermore, long-term stimulation of either A- or C-fiber baroreceptors is required to conclude that sustained reductions are mediated via C-fiber baroreceptor central pathways. However, given the very small involvement of A-fiber baroreceptor central pathways to the reduction of SNA after only 30 seconds and limited reduction in both SNA and AP during the 20 minute LVHf binary white noise stimulation protocol, it appears unlikely that A-fiber stimulation would be able to reduce SNA chronically. Examining electrical stimulation of A- and C-fiber baroreceptors in animal models of hypertension may be a possible future direction of study. Lastly, we also sectioned vagi to remove the influences of cardiopulmonary reflexes on SNA thus opening the arterial baroreflex negative feedback loop. Consequently, the transfer function of the Stim-AP arc does not include the vagal limb of the baroreflex. Further investigation is required to identify how selective stimulation of A- and C-fiber baroreceptors affects the vagal limb of the arterial baroreflex.

Conclusion

While device-based therapies that activate the arterial baroreflex have shown promising reductions in AP in resistant-hypertension patients the central pathways involved are still not entirely understood. This study highlights the two distinct baroreceptor pathways that need to be considered when investigating the role of the arterial baroreflex in the regulation of AP in health and disease. Furthermore, it indicates that electrical stimulation of C-fiber baroreceptors may be integral for a sustained reduction in AP, which is consistent with an increasingly large body of evidence that the arterial baroreflex can chronically inhibit SNA (Thrasher, 2005b; Lohmeier and Iliescu, 2011). A greater understanding of the integration and processing of the arterial baroreflex may also lead to novel ways of directly targeting either A- or C-fiber baroreceptor central pathways to chronically lower SNA and AP in hypertensive patients.

Grants

This study was supported by Health and Labour Sciences Research Grants (H19-nano-Ippan-009, H20-katsudo-Shitei-007, and H21-nano-Ippan-005) from the Ministry of Health, Labour and Welfare of Japan; Intramural Research Fund (25-6-17) of the National Cerebral and Cardiovascular Center; Grant-in-Aid for Scientific Research (JSPS KAKENHI Grant Number 23592319); and Grant-in-Aid for JSPS Fellows (JSPS KAKENHI Grant Number 2301705).

Conflict of interest

The authors declared no conflict of interest.

References

Bakris GL, Nadim MK, Haller H, Lovett EG, Schafer JE, Bisognano JD. Baroreflex activation therapy provides durable benefit in patients with resistant hypertension: results of long-term follow-up in the Rheos Pivotal Trial. J Am Soc Hypertens 2012;6:152–8.
Bendat JS, Piersol AG. Random data: analysis and measurement procedures. New Jersey: Wiley, Hoboken; 2010.
Brown AM, Saum WR, Yasui S. Baroreceptor dynamics and their relationship to afferent fiber type and hypertension. Circ Res 1978;42:694–702.
Chapleau MW, Lu J, Hajduczok G, Abboud FM. Mechanisms of baroreceptor adaptation in dogs: attenuation of adaptation by the K+ channel blocker 4-aminopyridine. J Physiol 1993;462:291–306.
Cowley Jr AW. Long-term control of arterial pressure. Physiol Rev 1992;72:231–300.
Fan W, Andresen MC. Differential frequency-dependent reflex integration of myelinated and nonmyelinated rat aortic baroreceptors. Am J Physiol Heart Circ Physiol 1998; 275:632–40.
Fan W, Schild JH, Andresen MC. Graded and dynamic reflex summation of myelinated and unmyelinated rat aortic baroreceptors. Am J Physiol Regul Integr Comp Physiol 1999; 277:748–56.
Fazan VP, Salgado HC, Barreira AA. Aortic depressor nerve unmyelinated fibers in spontaneously hypertensive rats. Am J Physiol Heart Circ 2001;4:1560–4.
Guyton AC. Arterial pressure and hypertension. Philadelphia, PA: Saunders; 1980.
Jones JV, Thoren PN. Characteristics of aortic baroreceptors with nonmedullated afferents arising from the aortic arch of rabbits with chronic renovascular hypertension. Acta Physiol Scand 1977;101:286–93.
Kawada T, Zheng C, Yanagiya Y, Uemura K, Miyamoto T, Inagaki M, Shishido T, Sugimachi M, Sunagawa K. High-cut characteristics of the baroreflex neural arc preserve baroreflex gain against pulsatile pressure. Am J Physiol Heart Circ Physiol 2002;282:1149–56.
Kawada T, Shimizu S, Kamiya A, Sata Y, Uemura K, Sugimachi M. Dynamic characteristics of baroreflex neural and peripheral arcs are preserved in spontaneously hypertensive rats. Am J Physiol Regul Integr Comp Physiol 2010;300:155–65.
Krieger EM. Neurogenic mechanisms in hypertension: resetting of the baroreceptors. Hypertension 1986;8:7–14.
Kubo T, Imaizumi T, Harasawa Y, Ando S, Tagawa T, Endo T, Shiramoto M, Takeshita A. Transfer function analysis of central arc of aortic baroreceptor reflex in rabbits. Am J Physiol Heart Circ Physiol 1996;39:1054–62.

Lohmeier TE, Iliescu R. Chronic lowering of blood pressure by carotid baroreflex activation: mechanisms and potential for hypertension therapy. Hypertension 2011;57:880–6.
Lohmeier TE, Iliescu R, Liu B, Henegar JR, Maric-Bilkan C, Irwin ED. Systemic and renal-specific sympathoinhibition in obesity hypertension. Hypertension 2012;59:331–8.
Numao Y, Siato M, Terui N, Kumada M. The aortic nerve-sympathetic reflex in the rat. J Auton Nerv Syst 1985;13:65–79.
Petiot E, Barrès C, Chapuis B, Julien C. Frequency response of renal sympathetic nervous activity to aortic depressor nerve stimulation in the anaesthetized rat. J Physiol 2001;537:949–59.
Reynolds PJ, Fan W, Andresen MC. Capsaicin-resistant arterial baroreceptors. J Negat Results Biomed 2006;5:6–15.
Stocker SD, Muntzel MS. Recording sympathetic nerve activity chronically in rats: surgery techniques, assessment of nerve activity, and quantification. Am J Physiol Heart Circ Physiol 2013;305:H1407–16.
Sun H, Li D, Chen S, Hittelman WN, Pan H. Sensing of blood pressure increase by transient receptor potential vanilloid 1 receptors on baroreceptors. J Pharmacol Exp Ther 2009;331:851–9.
Thoren P, Munch PA, Brown AM. Mechanisms for activation of aortic baroreceptor C-fibres in rabbits and rats. Acta Physiol Scand 1999;166:167–74.
Thrasher TN. Baroreceptors, baroreceptor unloading, and the long-term control of blood pressure. Am J Physiol Integr Comp Physiol 2005a;288:819–27.
Thrasher TN. Effects of chronic baroreceptor unloading on blood pressure in the dog. Am J Physiol Regul Integr Comp Physiol 2005b;288:863–71.

Heart Vessels
DOI 10.1007/s00380-014-0525-4

ORIGINAL ARTICLE

A novel technique to predict pulmonary capillary wedge pressure utilizing central venous pressure and tissue Doppler tricuspid/mitral annular velocities

Kazunori Uemura · Masashi Inagaki · Can Zheng · Meihua Li · Toru Kawada · Masaru Sugimachi

Received: 18 February 2014 / Accepted: 9 May 2014

Abstract Assessing left ventricular (LV) filling pressure (pulmonary capillary wedge pressure, PCWP) is an important aspect in the care of patients with heart failure (HF). Physicians rely on right ventricular (RV) filling pressures such as central venous pressure (CVP) to predict PCWP, assuming concordance between CVP and PCWP. However, the use of this method is limited because discordance between CVP and PCWP is observed. We hypothesized that PCWP can be reliably predicted by CVP corrected by the relationship between RV and LV function, provided by the ratio of tissue Doppler peak systolic velocity of tricuspid annulus (S_T) to that of mitral annulus (S_M) (corrected CVP:CVP·S_T/S_M). In 16 anesthetized closed-chest dogs, S_T and S_M were measured by transthoracic tissue Doppler echocardiography. PCWP was varied over a wide range (1.8–40.0 mmHg) under normal condition and various types of acute and chronic HF. A significantly stronger linear correlation was observed between CVP·S_T/S_M and PCWP ($R^2 = 0.78$) than between CVP and PCWP ($R^2 = 0.22$) ($P < 0.01$). Receiver-operating characteristic (ROC) analysis indicated that CVP·S_T/S_M >10.5 mmHg predicted PCWP >18 mmHg with 85 % sensitivity and 88 % specificity. Area under ROC curve for CVP·S_T/S_M to predict PCWP >18 mmHg was 0.93, which was significantly larger than that for CVP (0.66) ($P < 0.01$). Peripheral venous pressure (PVP) corrected by S_T/S_M (PVP·S_T/S_M) also predicted PCWP reasonably well, suggesting that PVP·S_T/S_M may be a minimally invasive alternative to CVP·S_T/S_M. In conclusion, our technique is potentially useful for the reliable prediction of PCWP in HF patients.

Keywords Heart failure · Hemodynamics · Echocardiography

K. Uemura (✉) · M. Inagaki · C. Zheng · M. Li · T. Kawada · M. Sugimachi
Department of Cardiovascular Dynamics, National Cerebral and Cardiovascular Center, 5-7-1 Fujishirodai, Suita 565-8565, Japan
e-mail: kuemura@ncvc.go.jp

Introduction

Assessing left ventricular (LV) filling pressure is an important aspect in the care of patients with heart failure (HF) [1]. The clinical gold standard for evaluating LV filling pressure is pulmonary capillary wedge pressure (PCWP) measured using pulmonary artery catheter. However, the invasive nature of catheterization limits its routine clinical use [2]. Noninvasive estimations of LV filling pressure by echocardiography have been developed [3–5]. However, the reliability of these methods in HF patients has been inconsistent [6, 7]. A minimally invasive and reliable method to estimate LV filling pressure has been keenly awaited.

In clinical practice, physicians rely on right ventricular (RV) filling pressures such as central venous pressure (CVP) to predict LV filling pressure, assuming concordance between the two filling pressures [8, 9]. However, the use of this method is limited because discordance between the two filling pressures has been observed in a substantial proportion of acute [10] or chronic [11, 12] HF patients. Physiologically, equality of stroke volumes (SV) of RV and LV is maintained by shifting of blood between the systemic and pulmonary vascular beds in accordance with the relation between RV and LV functions, which adjusts the two filling pressures [10, 13, 14]. If LV function is selectively impaired while RV function is spared, blood shifts from the systemic to pulmonary circuit to maintain

Published online: 31 May 2014

the equality of RV and LV SV, but discordance between the two filling pressures occurs (increased LV and decreased RV filling pressures) [10, 13, 14]. The relation between RV and LV functions may determine the relation between RV and LV filling pressures, i.e., the relation between CVP and PCWP.

Peak systolic tricuspid (S_T) [15–17] and mitral (S_M) [18–21] annular velocities measured by tissue Doppler echocardiography have been shown to sensitively reflect RV and LV systolic functions, respectively. Our theoretical analysis (see "Materials and methods") indicates that PCWP, CVP, S_T and S_M are related as follows:

$$\mathrm{PCWP} = \alpha \cdot \mathrm{CVP} \cdot S_T/S_M \quad (1)$$

where α is a constant. Based on Eq. 1, we hypothesized that CVP corrected by the relationship between RV and LV functions ($\mathrm{CVP}\cdot S_T/S_M$) reliably predicts PCWP. The primary purpose of this study was to validate this hypothesis. CVP is invasively measured by central venous catheterization, while peripheral venous pressure (PVP) is easily and safely measured [22]. PVP tightly correlates with CVP [23]. Hence, the secondary purpose of this study was to examine whether $\mathrm{PVP}\cdot S_T/S_M$ can be used as a minimally invasive alternative to $\mathrm{CVP}\cdot S_T/S_M$ in predicting PCWP. For these purposes, we conducted rigidly controlled experiments in canine models of acute and chronic HF over a wide preload range, which is not possible in humans.

Materials and methods

Theoretical analysis of the relation between PCWP, CVP, S_T and S_M

Assuming RV and LV SV are equal, ejection fraction of RV (RVEF) and LV (LVEF) are related to end-diastolic volumes of RV (RVEDV) and LV (LVEDV), respectively, as follows:

$$\mathrm{RVEF} = \mathrm{SV}/\mathrm{RVEDV} \quad (2)$$

$$\mathrm{LVEF} = \mathrm{SV}/\mathrm{LVEDV} \quad (3)$$

Dividing Eq. 2 by Eq. 3 and rearranging yields:

$$\mathrm{RVEF} \times \mathrm{RVEDV} = \mathrm{LVEF} \times \mathrm{LVEDV} \quad (4)$$

Based on previous studies [24, 25], we assume that RV filling pressure (CVP) and LV filling pressure (PCWP) are related to RVEDV and LVEDV, respectively, as follows:

$$\mathrm{CVP} = k_1 \cdot \mathrm{RVEDV} \quad (5)$$

$$\mathrm{PCWP} = k_2 \cdot \mathrm{LVEDV} \quad (6)$$

where k_1 and k_2 are constants.

S_T and S_M measured by tissue Doppler echocardiography have been shown to correlate well with RVEF [15, 16] and LVEF [18, 19], respectively, as follows,

$$S_T = k_3 \cdot \mathrm{RVEF} \quad (7)$$

$$S_M = k_4 \cdot \mathrm{LVEF} \quad (8)$$

where k_3 and k_4 are constants.

Substituting the four variables in Eq. 4 by Eqs. 5–8 and rearranging yields:

$$\mathrm{PCWP} = \frac{k_2 \cdot k_4}{k_1 \cdot k_3} \cdot \mathrm{CVP} \cdot S_T/S_M \quad (9)$$

If we define constant α as follows:

$$\alpha = \frac{k_2 \cdot k_4}{k_1 \cdot k_3} \quad (10)$$

PCWP, CVP, S_T and S_M are related as shown in Eq. 1.

Animals

We used 18 adult mongrel dogs (9 male and 9 female, 22 ± 2 kg). The investigation conformed to the *Guide for the Care and Use of Laboratory Animals* published by the US National Institutes of Health (NIH Publication No. 85-23, revised 1996). All protocols were approved by the Animal Subjects Committee of the National Cerebral and Cardiovascular Center.

Preparation

After anesthesia was induced with thiamylal sodium (25 mg kg^{-1}), the animals were intubated endotracheally, and their lungs were ventilated artificially. An appropriate level of anesthesia was maintained by continuous inhalation of 2.0 % isoflurane. A 6-F pulmonary artery catheter (T173HF6, Edwards Lifesciences, Irvine, CA) was positioned in the pulmonary artery through a 9-F sheath introducer placed in the right jugular vein. The pulmonary artery catheter and the side-port of the introducer were connected to pressure transducers (DX-200, Nihon Kohden, Tokyo, Japan) to measure PCWP and CVP, respectively. An 8-F sheath introducer was placed in the left carotid artery and the side-port was connected to a pressure transducer to measure systemic arterial pressure (AP). A 16-gauge catheter was placed in the right cephalic vein (a superficial vein of the right upper limb), and was connected to a pressure transducer to measure PVP. The animals were held in a standing position using a sling on a fluoroscopy table to allow continuous echocardiographic monitoring during cardiac catheterization and hemodynamic interventions [21, 26]. After being

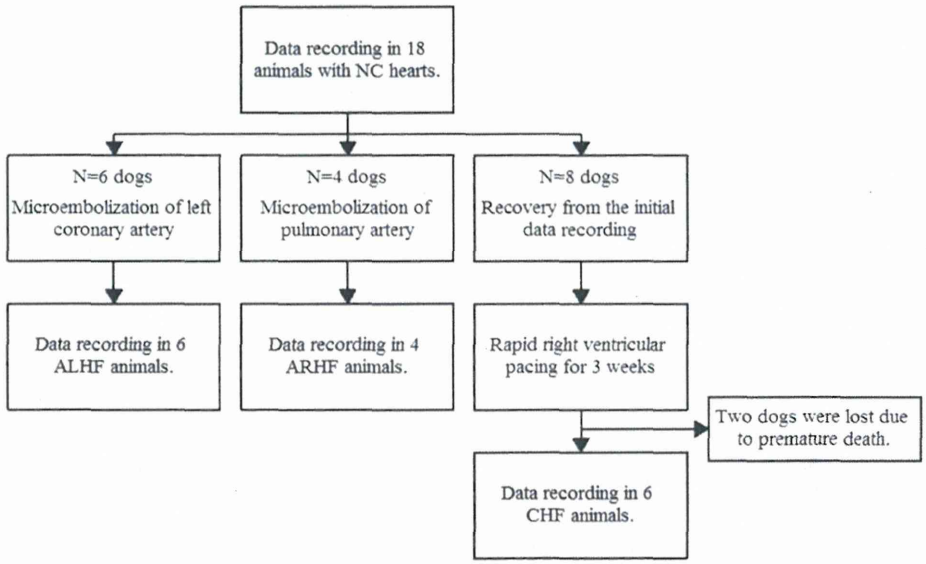

Fig. 1 Study protocol with intervention sequence and cardiac conditions. *NC* normal control, *ALHF* acute left heart failure, *ARHF* acute right heart failure, *CHF* chronic heart failure

connected to a pressure amplifier (AP-610J, Nihon Kohden, Tokyo, Japan), the pressure transducers were balanced at atmospheric pressure, calibrated against a mercury manometer, and zero referenced at the level of the mid-left ventricle under fluoroscopic guidance. Surface ECG was recorded. Hemodynamic data were acquired with the balloon of the pulmonary artery catheter inflated to measure PCWP, while the artificial ventilation was temporarily suspended at end-expiration. Analog signals of ECG, AP, CVP, PVP and PCWP were digitized (200 Hz, 16-bit) by a laboratory computer (ME-B, NEC, Tokyo, Japan), and stored on a hard disk for off-line analysis.

Echocardiographic examinations

Transthoracic echocardiography was performed using an echocardiographic system equipped with a 3.3-MHz transducer (Artida, Toshiba, Tokyo, Japan) [21, 26]. The transducer was directed from the apex to obtain an apical 4-chamber view, and fixed using a mechanical arm. Echocardiogram was recorded simultaneously with acquisition of hemodynamic data, while the artificial ventilation was temporarily suspended at end-expiration. The tricuspid and mitral annular velocities were obtained with pulsed tissue Doppler by placing 2-mm wide sample volumes at the free wall side of the tricuspid annulus [17] and mitral annulus [21], respectively. Transmitral inflow velocity was obtained with pulsed Doppler by placing a 3-mm wide sample volume between the tips of the opened mitral valve leaflets [27]. All Doppler tracings were recorded and stored on the internal hard drive of the echocardiographic system for off-line analysis.

Protocols

Study protocols are schematized in Fig. 1. In all 18 dogs, we first recorded the hemodynamic and echocardiographic data of nonfailing control hearts (NC). We increased preload by infusing 250 mL of 10 % dextran 40 gradually until mean CVP reached 9–11 mmHg. Simultaneous hemodynamic and echocardiographic recordings were repeated 5–7 times per animal, while volume administration was temporarily suspended to maintain steady-state pressures. After data acquisition in NC hearts, we withdrew blood to reduce mean CVP to 3–5 mmHg.

Subsequently, in 6 animals, acute left heart failure (ALHF) was induced by embolizing the left circumflex coronary artery with glass microspheres (90-μm diameter) [14, 21]. We adjusted the number of microspheres to increase mean PCWP by 18 mmHg. In 4 animals, acute right heart failure (ARHF) was induced by embolizing the pulmonary artery with glass microspheres [28], while the balloon of the pulmonary artery catheter was continuously inflated to monitor mean PCWP. We adjusted the number of microspheres to increase mean CVP by 9 mmHg. In ALHF and ARHF animals (Fig. 1), preload was varied by gradually infusing 250 mL of 10 % dextran 40 or withdrawing blood. Simultaneous hemodynamic and echocardiographic recordings were repeated 5–16 times per animal, in the same manner as described above.

In 8 animals, after the first recordings, the venous and arterial catheters were removed, the vessels were repaired, and the incisions were closed using sterile techniques. The animals were allowed to recover for 1 week (Fig. 1). Then, a pacemaker was implanted. Under general anesthesia as described above, a bipolar pacing lead (Model BT-45P,

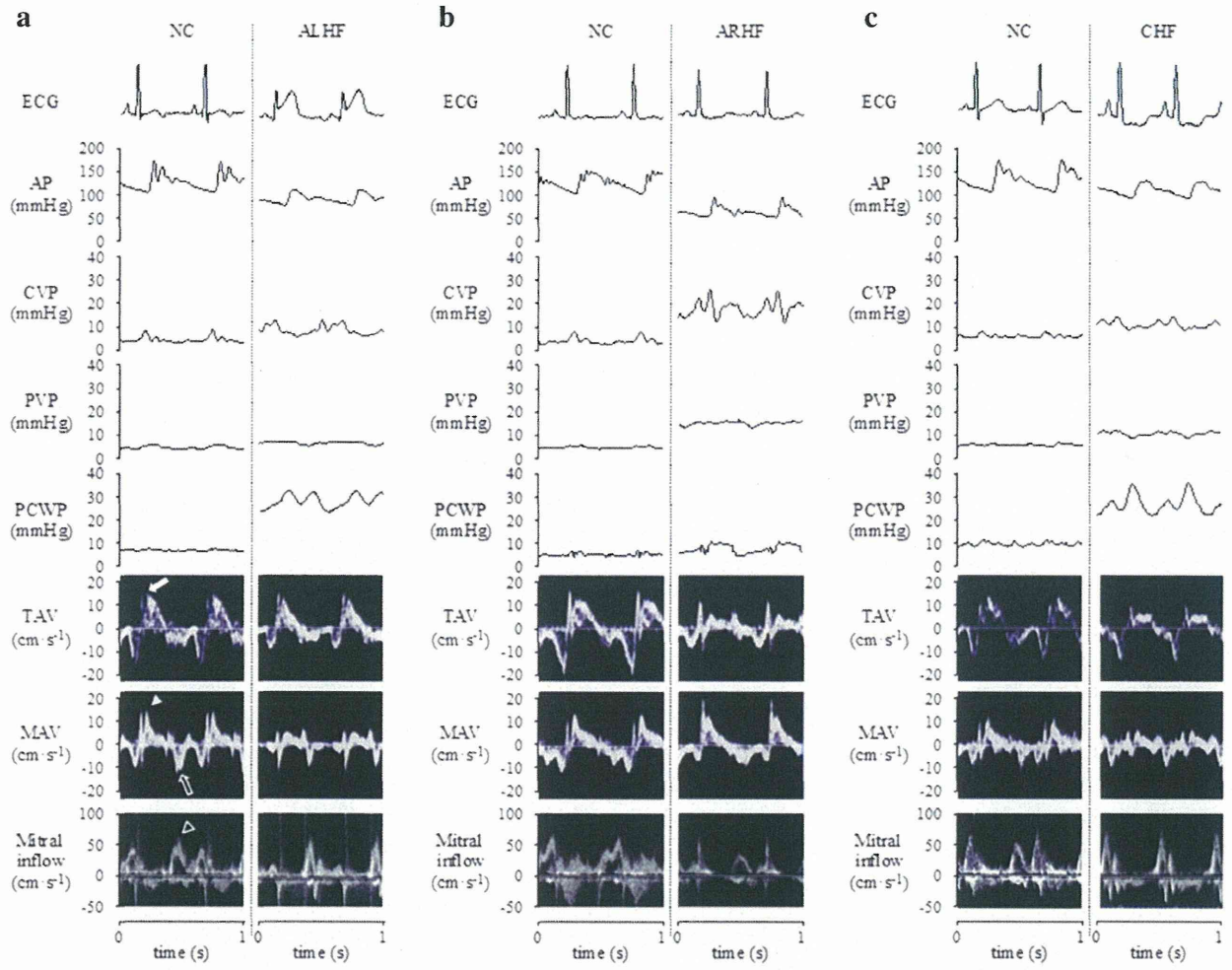

Fig. 2 Representative hemodynamic and echocardiographic tracings in animals allocated to ALHF (**a**), ARHF (**b**), and CHF (**c**) groups. *AP* arterial pressure, *CVP* central venous pressure, *PVP* peripheral venous pressure, *PCWP* pulmonary capillary wedge pressure, *TAV* tricuspid annular velocity, *MAV* mitral annular velocity. *Solid arrow* peak systolic tricuspid annular velocity (S_T), *solid arrow head* peak systolic mitral annular velocity (S_M), *open arrow* peak early diastolic mitral annular velocity (E_a), *open arrow head* peak early diastolic transmitral inflow velocity (E)

Star Medical Inc., Tokyo, Japan) was inserted through the right jugular vein, advanced to the right ventricular apex, and connected to a generator (VOO mode; Model SIP-501, Star Medical Inc., Tokyo, Japan), which was implanted in a subcutaneous pocket in the neck. The incisions were closed, and anesthesia was withdrawn. One day after implantation, rapid ventricular pacing was started at a rate of 220–240 beats/min and continued for 3 weeks to induce chronic biventricular HF (CHF) (Fig. 1) [29]. CHF was confirmed by the presence of HF symptoms including anorexia, lethargy, tachypnea and muscle weakening. After HF was confirmed, pacing was stopped. The CHF animals were anesthetized and prepared for hemodynamic and echocardiographic data recordings as described above. Preload was varied by gradually infusing 250 mL of 10 % dextran 40 or withdrawing blood. Simultaneous hemodynamic and echocardiographic recordings were repeated 5–8 times per animal, in the same manner as described above.

At the conclusion of the experiments, the dogs were euthanized with an intravenous injection of pentobarbital and potassium chloride.

Data analysis

Representative hemodynamic and echocardiographic tracings are shown in Fig. 2. We determined heart rate (HR) from the trace of ECG. AP, CVP, PVP and PCWP data were averaged over 10 s.

Peak velocities during systole of tricuspid annulus (S_T, solid arrow in Fig. 2a) and mitral annulus (S_M, solid arrow

head in Fig. 2a) as well as peak early diastolic velocities of mitral annulus (E_a, open arrow in Fig. 2a) and transmitral inflow (E, open arrow head in Fig. 2a) were measured using a digital Doppler analysis system. Data of echocardiographic variables were expressed as the averages of 3 consecutive cardiac cycles. All echocardiographic analyses were performed off-line by a trained cardiologist (MI) blinded to the hemodynamic data.

Multiple datasets of HR, AP, CVP, PVP, PCWP, S_T, S_M, S_T/S_M, CVP·S_T/S_M PVP·S_T/S_M, E, E_a and E/E_a were determined in each animal. We also calculated absolute changes in PCWP (ΔPCWP), CVP (ΔCVP), CVP·S_T/S_M (ΔCVP·S_T/S_M), PVP·S_T/S_M (ΔPVP·S_T/S_M) and E/E_a (ΔE/E_a) between serial measurements within each animal.

Statistical analysis

All data are presented as mean ± SD. One-way ANOVA with Dunnett's test was used in multiple comparisons for each HF condition relative to NC. Linear regression analysis and the coefficient of determination (R^2) were used to determine the strength of association among the variables. Receiver-operating characteristic (ROC) curve analysis was used to determine optimal cutoff values for selected variables to detect PCWP >18 and >22 mmHg [30]. The area under the ROC curve (AUC) was determined as a summary measure for diagnostic accuracy of the variables. Since accurate estimation of serial changes in PCWP in response to therapy is also important in clinical practice, ROC curve analysis was performed to determine optimal cutoff values for selected variables to predict ΔPCWP >3 and <−3 mmHg. To compare R^2 value of each correlation and AUC of each ROC curve, we used a bootstrap technique (200 replicates) [20, 31]. A P value <0.05 was considered statistically significant. Statistical analyses were performed using commercially available software (Statistica, Statsoft, Inc., Tulsa, OK, USA).

Results

In the 18 dogs, 2 dogs in CHF protocol developed ventricular fibrillation during rapid ventricular pacing, and died before completion of the protocol. From other 16 dogs (6 ALHF, 4 ARHF and 6 CHF dogs), a total of 243 datasets of hemodynamic and echocardiographic variables were obtained (Table 1). We used the datasets to validate the hypothesis that CVP·S_T/S_M reliably predicts PCWP. We compared prediction of PCWP by CVP·S_T/S_M to that by CVP alone.

Of the 16 dogs, PVP data were not available for 3 dogs due to technical errors. From the 13 remaining dogs (5 ALHF, 3 ARHF and 5 CHF dogs), a total of 195 datasets of hemodynamic and echocardiographic variables were obtained (Table 2). We used the datasets to examine whether PVP·S_T/S_M can be used as a minimally invasive alternative to CVP·S_T/S_M in predicting PCWP. We compared prediction of PCWP by PVP·S_T/S_M to that by E/E_a, which is commonly used in clinical practice [3–5].

Range of PCWP achieved in this study (Tables 1, 2) is similar to that seen in advanced HF patients [11].

Prediction of PCWP by CVP·S_T/S_M

In ALHF (Table 1; Fig. 2a), PCWP and CVP were significantly higher, S_T was slightly but significantly lower, S_M was significantly lower, and S_T/S_M was significantly higher than the corresponding values in NC. In ARHF (Table 1; Fig. 2b), CVP but not PCWP was significantly higher, S_T was significantly lower, S_M was significantly higher, and S_T/S_M was significantly lower than the corresponding values in NC. In CHF (Table 1; Fig. 2c), PCWP and CVP were significantly higher, S_T and S_M were significantly lower, and S_T/S_M was significantly higher than the corresponding values in NC. CVP·S_T/S_M was significantly higher in all HF conditions than in NC (Table 1).

A significant but weak correlation was observed between CVP and PCWP (Fig. 3a), while a strong correlation was found between CVP·S_T/S_M and PCWP (Fig. 3b). The R^2 value between CVP·S_T/S_M and PCWP was significantly higher than that between CVP and PCWP ($P < 0.01$). A significant and strong correlation was observed between ΔCVP and ΔPCWP, and also between ΔCVP·S_T/S_M and ΔPCWP (Fig. 3c, d). The R^2 value between ΔCVP·S_T/S_M and ΔPCWP was significantly higher than that between ΔCVP and ΔPCWP ($P < 0.05$).

The ROC curves for CVP and CVP·S_T/S_M in predicting PCWP >18 mmHg are shown in Fig. 3e. The optimal cutoff values were >7.0 mmHg (sensitivity, 72 %; specificity, 57 %) for CVP, and >10.5 mmHg (sensitivity, 85 %; specificity, 88 %) for CVP·S_T/S_M. The ROC curve for CVP·S_T/S_M lay entirely above the curve for CVP. The AUC for CVP·S_T/S_M was significantly larger than that for CVP ($P < 0.01$) (Fig. 3e). ROC analyses of these variables to detect PCWP >22 mmHg (Fig. 3f) yielded similar results. The AUC for CVP·S_T/S_M was significantly larger than that for CVP ($P < 0.01$).

The ROC curves for ΔCVP and ΔCVP·S_T/S_M in predicting ΔPCWP >3 mmHg are shown in Fig. 3g. The optimal cutoff values were >1.0 mmHg (sensitivity, 86 %; specificity, 73 %) for ΔCVP, and >2.0 mmHg (sensitivity, 89 %; specificity, 85 %) for ΔCVP·S_T/S_M. The AUC for ΔCVP and for ΔCVP·S_T/S_M were similar. ROC analyses of these variables to predict ΔPCWP <−3 mmHg (Fig. 3h) produced similar results. The AUC for ΔCVP and for ΔCVP·S_T/S_M were similar.

Table 1 Hemodynamic and echocardiographic data used to evaluate CVP·S_T/S_M

	All datasets ($n = 243$)	Subgroups			
		NC ($n = 94$)	ALHF ($n = 68$)	ARHF ($n = 41$)	CHF ($n = 40$)
HR, bpm	109 ± 13 (71 to 156)	106 ± 14	111 ± 9	102 ± 7	119 ± 17*
AP, mmHg	114 ± 21 (60 to 155)	130 ± 16	98 ± 13*	100 ± 19*	113 ± 7*
CVP, mmHg	7.9 ± 4.0 (−0.5 to 19.4)	5.7 ± 3.3	7.5 ± 2.6*	11.8 ± 2.9*	9.9 ± 4.4*
PCWP, mmHg	17.5 ± 9.2 (1.8 to 40.0)	11.0 ± 5.3	24.4 ± 5.9*	10.3 ± 2.5	28.1 ± 6.6*
S_T, cm/s	11.9 ± 2.9 (5.2 to 21.5)	13.3 ± 2.8	12.1 ± 2.2*	10.6 ± 2.3*	9.7 ± 2.8*
S_M, cm/s	9.4 ± 3.8 (3.4 to 17.6)	11.4 ± 2.8	5.8 ± 1.2*	13.6 ± 2.2*	6.3 ± 1.5*
S_T/S_M	1.5 ± 0.6 (0.5 to 3.4)	1.2 ± 0.3	2.2 ± 0.5*	0.8 ± 0.2*	1.5 ± 0.4*
CVP·S_T/S_M, mmHg	11.1 ± 6.4 (−0.9 to 31.5)	6.7 ± 4.0	16.0 ± 6.2*	9.3 ± 2.9*	14.7 ± 6.2*

Values are presented as mean ± SD (range)

NC normal control, *ALHF* acute left heart failure, *ARHF* acute right heart failure, *CHF* chronic heart failure, *HR* heart rate, *AP* systemic arterial pressure, *CVP* central venous pressure, *PCWP* pulmonary capillary wedge pressure, S_T peak systolic tricuspid annular velocity, S_M peak systolic mitral annular velocity

* $P < 0.01$ against NC

Table 2 Hemodynamic and echocardiographic data used to evaluate PVP·S_T/S_M

	All datasets ($n = 195$)	Subgroups			
		NC ($n = 75$)	ALHF ($n = 59$)	ARHF ($n = 29$)	CHF ($n = 32$)
CVP, mmHg	7.9 ± 3.9 (−0.5 to 19.4)	5.8 ± 3.3	7.7 ± 2.5†	12.2 ± 3.0†	9.5 ± 4.4†
PVP, mmHg	7.7 ± 3.5 (−0.5 to 17.3)	6.4 ± 3.0	6.9 ± 2.3	11.9 ± 2.4†	8.4 ± 4.1†
PCWP, mmHg	18.0 ± 9.4 (1.8 to 40.0)	11.0 ± 5.2	25.0 ± 5.8†	10.7 ± 2.4	28.3 ± 6.7†
CVP·S_T/S_M, mmHg	11.4 ± 6.6 (−0.9 to 31.5)	6.6 ± 3.9	16.7 ± 6.1†	9.5 ± 2.9*	14.4 ± 6.3†
PVP·S_T/S_M, mmHg	10.9 ± 5.7 (−0.6 to 28.7)	7.6 ± 4.0	15.0 ± 5.9†	9.4 ± 2.9	12.6 ± 5.3†
E, cm/s	60 ± 14 (30 to 101)	60 ± 14	59 ± 9	52 ± 10*	70 ± 16†
E_a, cm/s	9.5 ± 2.5 (4.3 to 15.6)	9.8 ± 2.8	8.0 ± 1.3†	11.6 ± 1.5†	9.5 ± 2.2
E/E_a	6.7 ± 1.9 (2.9 to 12.3)	6.4 ± 2.1	7.5 ± 1.1†	4.6 ± 0.9†	7.5 ± 1.4†

Values are presented as mean ± SD (range)

PVP peripheral venous pressure, *E* peak early diastolic transmitral flow velocity, E_a peak early diastolic mitral annular velocity

* $P < 0.05$, † $P < 0.01$ against NC

Minimally invasive prediction of PCWP by PVP·S_T/S_M

PVP·S_T/S_M and PCWP were correlated significantly and tightly (Fig. 4a), while a weak correlation was found between E/E_a and PCWP (Fig. 4b). The R^2 value between PVP·S_T/S_M and PCWP was significantly higher than that between E/E_a and PCWP ($P < 0.01$). A significant and tight correlation was observed between ΔPVP·S_T/S_M and ΔPCWP (Fig. 4c), while a weak correlation was observed between $\Delta E/E_a$ and ΔPCWP (Fig. 4d). The R^2 value between ΔPVP·S_T/S_M and ΔPCWP was significantly higher than that between $\Delta E/E_a$ and ΔPCWP ($P < 0.01$).

The ROC curves for PVP·S_T/S_M and E/E_a in predicting PCWP >18 mmHg are shown in Fig. 4e. The optimal cutoff values were >10.5 mmHg (sensitivity, 73 %; specificity, 84 %) for PVP·S_T/S_M, and >6.0 (sensitivity, 93 %; specificity, 66 %) for E/E_a. The AUC for PVP·S_T/S_M was larger than that for E/E_a with a clear tendency to significance ($P = 0.06$). The ROC curves for these variables in predicting PCWP >22 mmHg are shown in Fig. 4f. The optimal cutoff values were >11.5 mmHg (sensitivity, 72 %; specificity, 79 %) for PVP·S_T/S_M, and >6.5 (sensitivity, 81 %; specificity, 62 %) for E/E_a. The AUC for PVP·S_T/S_M was significantly larger than that for E/E_a ($P < 0.05$).

The ROC curves for ΔPVP·S_T/S_M and $\Delta E/E_a$ in predicting ΔPCWP >3 mmHg are shown in Fig. 4g. The optimal cutoff values were >1.5 mmHg (sensitivity, 90 %; specificity, 78 %) for ΔPVP·S_T/S_M, and >0.0 mmHg (sensitivity, 61 %; specificity, 56 %) for $\Delta E/E_a$. The AUC for ΔPVP·S_T/S_M was significantly larger than that for $\Delta E/E_a$ ($P < 0.01$). ROC analyses of these variables to predict ΔPCWP <−3 mmHg (Fig. 4h) produced similar results. The AUC for ΔPVP·S_T/S_M was significantly larger than that for $\Delta E/E_a$ ($P < 0.01$).

Discussion

The present results validate our hypothesis that CVP·S_T/S_M reliably predicts PCWP, and also suggest that PVP·S_T/S_M may be used as a minimally invasive alternative to CVP·S_T/S_M. To the best of our knowledge, we have for the first time

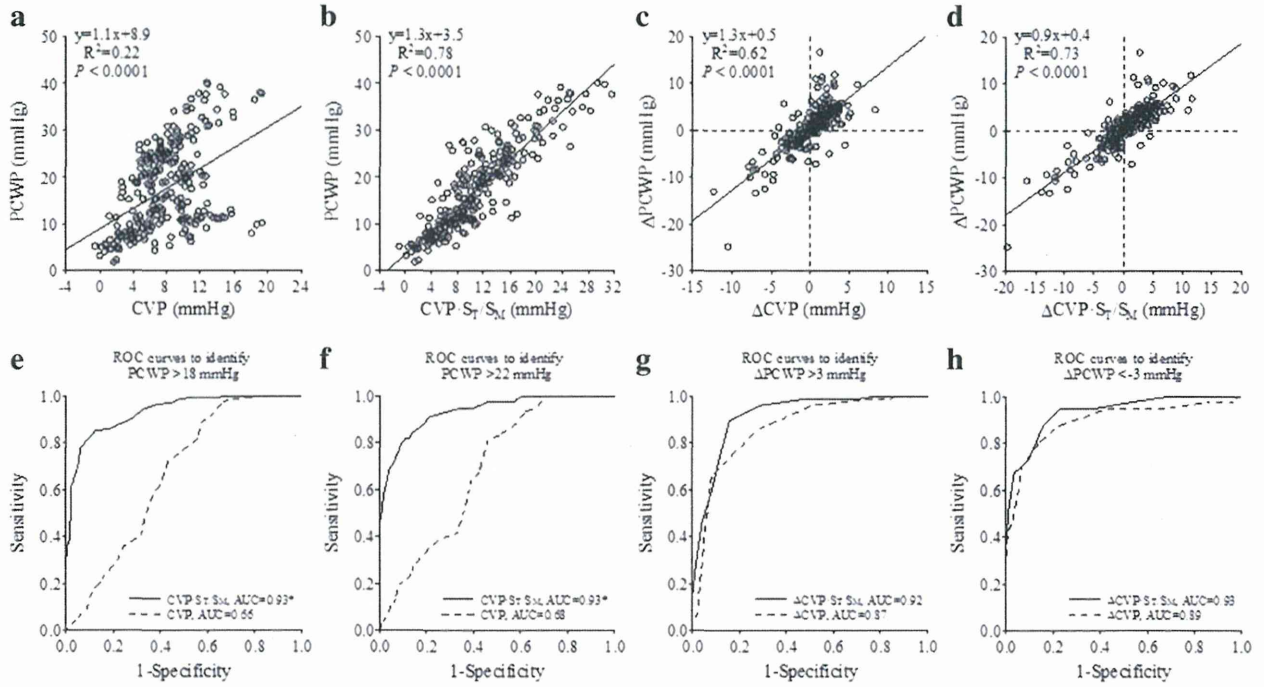

Fig. 3 Relationships between PCWP and CVP (**a**), PCWP and CVP·S_T/S_M (**b**) (243 datasets analyzed). Relationships between serial changes in PCWP (ΔPCWP) and serial changes in CVP (ΔCVP) (**c**), ΔPCWP and serial changes in CVP·S_T/S_M (ΔCVP·S_T/S_M) (**d**) (227 data points analyzed). In panels **a–d**, the regression line, regression equation, coefficient of determination (R^2) and probability value are shown. Receiver-operating characteristic (ROC) curves for the prediction of PCWP >18 mmHg (**e**) and >22 mmHg (**f**) from CVP and CVP·S_T/S_M (243 datasets analyzed). ROC curves for the prediction of ΔPCWP >3 mmHg (**g**) and <−3 mmHg (**h**) from ΔCVP and ΔCVP·S_T/S_M, (227 data points analyzed). AUC indicates area under curve. * $P < 0.01$ versus CVP

successfully integrated the measurement of the venous pressure with echocardiographic assessment of cardiac function to predict PCWP. Indeed, over a wide range of preload, the correlation between CVP·S_T/S_M and PCWP is strong, and better than that between CVP and PCWP. CVP·S_T/S_M predicts abnormal elevation of PCWP more accurately than CVP. The ROC curves for CVP·S_T/S_M to predict abnormal elevation of PCWP and absolute changes in PCWP both had AUC exceeding 0.9, indicating excellent diagnostic accuracy [32]. The correlation between PVP·S_T/S_M and PCWP is tight, and better than that between E/E_a and PCWP. PVP·S_T/S_M predicts abnormal elevation of PCWP reasonably well, and absolute changes in PCWP more accurately than E/E_a. These findings suggest that our technique may be useful not only for the initial single time-point evaluation but also for continuous serial monitoring of PCWP to titrate diuretic or volume loading therapy in the management of HF patients.

S_T/S_M ratio reflects the relationship between RV and LV systolic functions

The S_T/S_M ratio in each HF condition reflected the pathological imbalance between RV and LV functions reasonably well. S_T/S_M was higher in ALHF and lower in ARHF compared to NC (Table 1). Although the pacing-induced CHF model is known to have severe biventricular dysfunction [29], S_T/S_M was significantly higher in CHF animals than that in NC. In this CHF model, LV function may have been more severely depressed relative to RV function. In each HF condition, the pathological imbalance between RV and LV functions was accompanied by a shift of blood between the systemic and pulmonary circuits. When the data in Fig. 3a are classified by cardiac conditions as shown in Fig. 5a, it is clear that for a given CVP, PCWP increases in ALHF and CHF but decreases in ARHF compared to NC. These indicate a shift of blood from the systemic to pulmonary circuits in ALHF and CHF, and in opposite direction in ARHF [10, 13, 14]. As shown in Fig. 5b, correcting CVP by the S_T/S_M ratio (CVP·S_T/S_M) improves the concordance with PCWP irrespective of cardiac conditions. Taken together, although the theoretical model of the relationship between PCWP, CVP, S_T and S_M in Eq. 1 is rather simple, it is both highly predictive and intuitively reasonable.

The assumption that S_T and S_M are related with RVEF [15, 16] and LVEF [18, 19], respectively (Eqs. 7 and 8 in "Materials and methods"), is valid. Our previous study

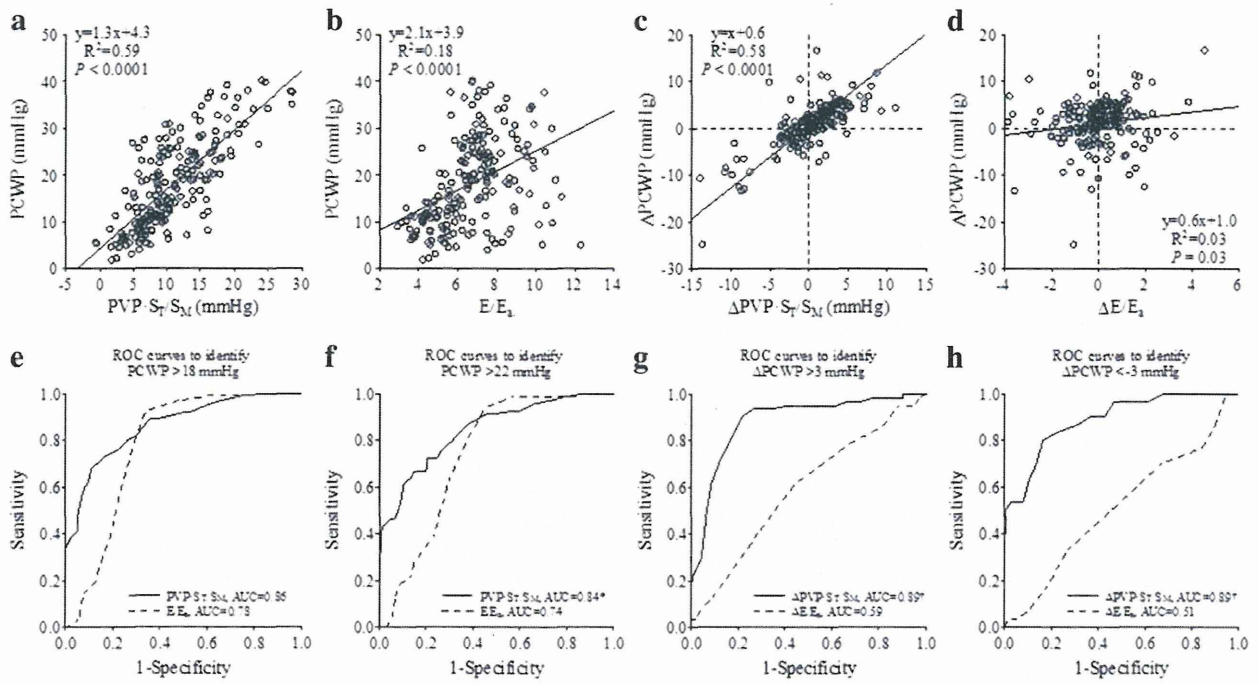

Fig. 4 Relationships between PCWP and PVP·S_T/S_M (**a**), PCWP and E/E_a (**b**) (195 datasets analyzed). Relationships between ΔPCWP and serial changes in PVP·S_T/S_M (ΔPVP·S_T/S_M) (**c**), ΔPCWP and serial changes in E/E_a ($\Delta E/E_a$) (**d**) (182 data points analyzed). In panels **a**–**d**, the regression line, regression equation, coefficient of determination (R^2) and probability value are shown. ROC curves for the prediction of PCWP >18 mmHg (**e**) and >22 mmHg (**f**) from PVP·S_T/S_M and E/E_a (195 datasets analyzed). ROC curves for the prediction of ΔPCWP >3 mmHg (**g**) and <−3 mmHg (**h**) from ΔPVP·S_T/S_M and $\Delta E/E_a$, (182 data points analyzed). * $P < 0.05$ versus E/E_a. † $P < 0.01$ versus $\Delta E/E_a$

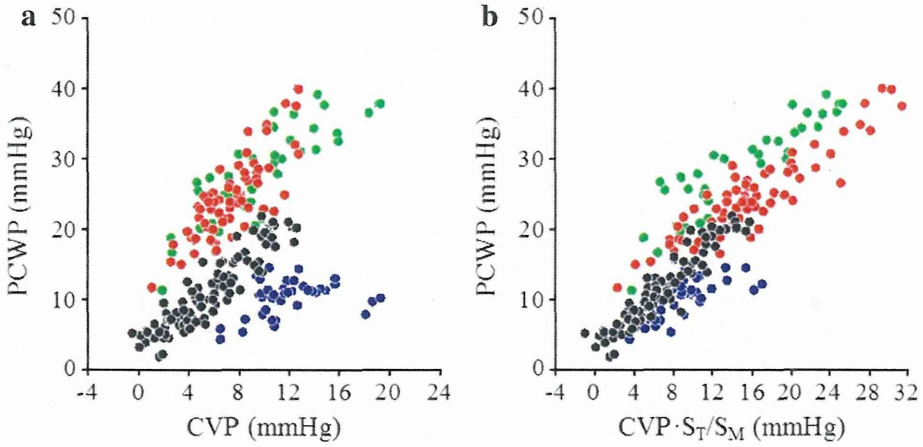

Fig. 5 Relationships of PCWP and CVP (**a**), PCWP and CVP·S_T/S_M (**b**). Each panel shows raw data from all 243 datasets. *Black dot* indicates NC, *red dot* ALHF, *blue dot* ARHF, *green dot* CHF

[21] demonstrated that S_M strongly reflects the status of left ventricular–arterial coupling, which also determines LVEF. S_M itself was not affected by LV preload over a wide range [21].

S_T/S_M ratio can be a clinically useful parameter reflecting the relation between RV and LV systolic function in various types of HF. Some previous results potentially supported this concept. Bruhl et al. [33] demonstrated that S_T/S_M ratio is reproducible and stable across age, body size and gender in a healthy adult population with no cardiac diseases. More interestingly, decreased S_T/S_M ratio predicted pulmonary embolism in patients with HF [34]. Our theoretical analysis (see "Materials and methods") suggests that instead of S_T/S_M ratio, the RVEF to LVEF ratio may be used as a parameter reflecting the relationship between RV and LV functions. However, the EF ratio may